Journal of Power Sources 196 (2011) 4162–4172

Contents lists available at ScienceDirect

Journal of Power Sources

journal homepage: www.elsevier.com/locate/jpowsour

Elucidation of electrochemical properties of electrolyte-impregnated micro-porous ceramic films as framework supports in dye-sensitized solar cells

Hseng Shao Chen [a], Shingjiang Jessie Lue [a,*], Yung Liang Tung [b], Kong Wei Cheng [a], Fu Yuan Huang [a], Kuo Chuan Ho [c]

[a] Department of Chemical and Materials Engineering and Green Technology Research Center, Chang Gung University, Kwei-shan, Taoyuan, 333 Taiwan
[b] Photovoltaics Technology Center, Industrial Technology Research Institute (ITRI), Hsin-Chu, 310 Taiwan
[c] Department of Chemical Engineering, National Taiwan University, Taipei, 106 Taiwan

ARTICLE INFO

Article history:
Received 10 October 2010
Received in revised form 6 December 2010
Accepted 7 December 2010
Available online 14 December 2010

Keywords:
Limiting current density
Tri-iodide diffusion coefficient
Porosity
Electrolyte-filled micro-porous framework
Cell performance

ABSTRACT

This study investigates the electrochemical properties of electrolyte-impregnated micro-porous ceramic (Al_2O_3) films as framework supports in dye-sensitized solar cells (DSSCs). A field-emission scanning electron microscope (FE-SEM) is used to characterize the morphology on both surfaces of the ceramic membranes, which exhibit high porosity (41–66%) and an open cylindrical pore structure. Electrochemical impedance analysis reveals that the conductivity of the electrolyte-impregnated ceramic membrane is lower (6.24–9.39 mS cm^{-1}) than the conductivity of the liquid electrolyte (25 mS cm^{-1}), with an Archie's relationship by a power of 1.81 to the porosity value. The diffusivity of tri-iodide ions (I_3^-) is slowed from 1.95×10^{-5} to 0.68×10^{-5} cm^2 s^{-1} in the ceramic-containing cells. The exchange current density at the Pt-electrolyte interface decreases slightly (less than 5%) when the Al_2O_3 membranes were used in the symmetric cells, implies that the contact of the denser ceramic top structure on the Pt electrode does not interfere with the I_3^- charge transfer. The ceramic films can prevent solvent evaporation and maintain conductivity. The long-term cell efficiencies are evaluated up to 1248 h under alternating light soaking and darkness (3 days/4 days) cycles. The cells containing the ceramic films outperform the control cells.

1. Introduction

Many countries and regions are focusing on the development of renewable energy to satisfy their present and future energy demands. Among various energy sources, photovoltaic cells are gaining much attention due to their low production costs and high energy-conversion efficiencies. Silicon-based solar cells have been manufactured on a large scale, and their installation is encouraged by many governments and nations. However, their high manufacturing costs spur the development of other types of solar cells. The manufacturing of dye-sensitized solar cells (DSSCs) is considered an inexpensive alternative [1,2] to the manufacturing of traditional silicon-based cells. However, the challenges in DSSCs, such as improving the material durability and prolonging cell lifetime, need to be resolved for future commercialization. Solvent loss and leakage due to the volatility of the organic solvent in the electrolyte is the main factor governing the DSSC's lifetime.

In recent years, many studies have focused on improving the stability of liquid electrolytes using other materials to avoid these major problems and to improve the performance of the cell. These efforts include the introduction of quasi-solid state electrolytes [3], ionic liquids [4], and porous membranes [5–9] into DSSCs. The ion diffusivity is slower in the solid electrolytes and ionic liquids than in the liquid state. Therefore, micro-porous films seem to have potential as the framework material due to their ability to retain solvent with the capillary force exerted between the porous support and liquid. Kim et al. fabricated a DSSC with a crylonitrile-methyl methacrylate co-polymer membrane with a high porosity (51%) and large film thickness (50–60 μm) [5]. A low photovoltaic efficiency of 2.4% (under 100 mW cm^{-2} illumination) was obtained. Zhang et al. prepared a DSSC with a smaller area (0.15 cm^2 compared with 0.25–0.28 cm^2 in other studies) and reported the conversion efficiency of the DSSC with gel membrane to be 6.0% at an irradiance of 75 mW cm^{-2}, which was still a lower efficiency than that of a liquid electrolyte cell (8.6%) [8]. Chen et al. reported a conversion efficiency of 4.58% with a poly(styrene-methyl methacrylate) blend and a film thickness of only 1.66 μm [6]. Park et al. employed liquid impregnated polymer membranes into the DSSC, forming quasi-solid-state electrolytes for a highly efficient DSSC with an overall conversion efficiency of 8% at room temperature under 1 sun illumination [9]. The framework materials exhibit various pore sizes, porosities, geometries, and levels of pore inter-connectivity. The electrochemical characteristics in the electrolyte-containing porous frameworks, however, are limited.

* Corresponding author. Tel.: +886 3 2118800x5489; fax: +886 3 2118700.
E-mail address: jessie@mail.cgu.edu.tw (S.J. Lue).

0378-7753/$ – see front matter © 2010 Elsevier B.V. All rights reserved.
doi:10.1016/j.jpowsour.2010.12.004

Nomenclature

$C_{I_3^-}$	concentration of tri-iodide (mol L^{-1})
$D_{I_3^-}$	diffusion coefficient of tri-iodide ($cm^2\ s^{-1}$)
F	Faraday constant (C mol^{-1})
FF	fill factor
J	current density (mA cm^{-2})
J_{lim}	limiting current density (mA cm^{-2})
J_0	exchange current density (mA cm^{-2})
J_{sc}	short-circuit density (mA cm^{-2})
l	cell gap (cm)
m	Archie's parameter
n	charge transfer number in redox reaction
P_{in}	incident light power (mW cm^{-2})
R	ideal gas constant (J $mol^{-1}\ K^{-1}$)
R_{ct}	charge transfer resistance ($\Omega\ cm^2$)
T	absolute temperature (K)
V_{oc}	open-circuit voltage (V)

Greek symbols

η	photo-to-current efficiency
σ	conductivity of electrolyte (S cm^{-1})
σ_{eff}	effective conductivity (S cm^{-1})
ε	porosity of membrane

This information is critical for the design and fabrication of porous framework materials.

In our previous study on the long-term performance of DSSCs (up to 1000 h) we found that the cell performance and percentage of viable cells were greatly improved by incorporating micro-porous polycarbonate films into the cell as an electrolyte framework support [10]. The present study aims to apply micro-porous ceramic (Al_2O_3) membranes as the electrolyte framework support for DSSCs and to investigate their electrochemical properties in a symmetric cell. The ceramic membrane exhibited a pseudo-straight cylindrical pore geometry similar to that exhibited by the track-etched polycarbonate film [11], but with higher porosity. The higher porosity may facilitate higher ion transport than other micro-porous membranes containing tortuous pore paths formed by the phase inversion method. In this work, the electrolyte solvent evaporation rate, charge transfer resistance, and diffusivity of tri-iodide ions (I_3^-) are correlated with the pore morphology of the inorganic films. The limiting current density and exchange current density are determined and correlated with the intrinsic characteristics of the electrolyte-impregnated Al_2O_3 films. Finally, the photo-to-current efficiencies of the as-prepared DSSCs and those aged under alternating light soaking and darkness cycles are evaluated.

2. Experimental

2.1. Materials

Ruthenium 535 bis-TBA (N719) dye was purchased from Dyesol Ltd., Queanbeyan, Australia. Acetonitrile (AN), iodine (I_2, 99.9% pure), and isopropyl alcohol (IPA) were obtained from J.T. Baker (Philipsburg, NJ, USA). Tert-butanol (99% pure), lithium iodide hydrate (LiI, 99.99% pure), 4-tert-butylpyridine (TBP, 99% pure) and hydrogen hexachloroplatinate (IV) hydrate (H_2PtCl_6) were obtained from Aldrich (St. Louis, MO, USA). 1-Methyl-3-propylimidazolium iodide (PMII) was synthesized by the Photovoltaic Technology Center at the Industrial Technology Research Institute (ITRI) in Hsin-Chu, Taiwan. Fluorine-doped tin oxide (FTO) conductive glass was from NSG America Inc., Somerset, NJ, USA. Hot melt sealing foil (SX1170-60) was obtained from Solaronix SA (Aubonne, Switzerland). A photo-curing compound (GN435) was purchased from Everwide Chemical Co. Ltd., Douliou, Taiwan. The micro-porous Al_2O_3 ceramic membranes (Whatman International Ltd., Anodisc, Maidston, England) with different nominal pore sizes of 0.2, 0.1, and 0.02 μm were used as electrolyte supports.

2.2. Al_2O_3 ceramic film characterization

The membrane morphologies of the ceramic supports with different pore sizes were studied using field-emission scanning electron microscopy (FE-SEM, model S-4800, Hitachi Ltd., Tokyo, Japan). An accelerating voltage of 20 kV and a current of 75 μA were used during the operation. The obtained micrographs were used to determine the porosity, average pore size and pore size distribution after being evaluated with image analysis software (SimplePCI, Hamamatsu Corp. Sewickley, PA, USA). The conductivities of the electrolyte-impregnated ceramic membranes were measured by electrochemical impedance analysis with a potentiostat (pgstat3, Autolab, Utrecht, Netherlands) with frequencies ranging from 10^6 to 10^{-2} Hz and an amplitude of 10 mV at 25 °C. The resistance data were extracted from the Nyquist plots and converted into conductivity values [12].

2.3. Symmetric cell preparation

Fluorine-doped tin oxide (FTO) conductive glass of $2.5 \times 1.5\ cm^2$ was used as the electrode substrate. Two platinum (Pt) electrodes were coated by dripping H_2PtCl_6 (0.015 M in IPA) on the clean FTO glass. One of the glass plates was drilled with two holes, 8 mm apart, prior to dripping the H_2PtCl_6 solution. The Pt electrodes were annealed at 400 °C for 20 min and then gradually cooled to room temperature for 10 min. The Pt exhibited a crystal structure, and it uniformly coated the FTO substrate, as shown in Fig. 1(a) and (b). The Al_2O_3 ceramic membrane was then carefully aligned and sandwiched between the two Pt electrodes with the Pt sides facing the ceramic film. A hot melt sealing foil was applied to seal the symmetric cell (as shown in Fig. 2(a)) using a hot press at 130 °C for 35 s under a pressure of 55 kN cm^{-2}. The electrolyte solution (0.6 M PMII/0.05 M I_2/0.1 M LiI/0.5 M TBP in AN) was injected into the cell gap through one drilled hole on the Pt electrode. The holes were sealed by ultraviolet (UV) light irradiation after a photo-curing compound was placed in the holes and covered by a slide glass (Fig. 2(a)). The symmetric cell was used for charge transfer resistance, I_3^- diffusivity measurements, and in the solvent evaporation test.

2.4. DSSC assembly

The FTO conductive glass of $2.5 \times 1.5\ cm^2$ was also used as the working electrode substrate. Photo-catalytic TiO_2 paste was synthesized and screen-printed onto the FTO substrate with an active area of 0.28 cm^2. The electrode was annealed at 400 °C for 20 min and cooled to room temperature. The morphology of the synthesized TiO_2 crystals is shown in Fig. 1(c) and (d). The electrode was then immersed in an N719 dye solution of 5×10^{-4} M in acetonitrile/tert-butanol (1:1 v/v) solution at atmospheric temperature for 24 h to adsorb the dye molecules. The electrode was rinsed with acetone to remove the excess dye solution and dried at 80 °C for 2 min.

The FTO with TiO_2 electrode, the Al_2O_3 ceramic membrane, and the counter Pt-electrode with two drilled holes (as prepared in the previous section) were carefully aligned. Two pieces of hot melt sealing foil were used to seal the DSSC cell using hot-press at 130 °C for 35 s under 55 kN cm^{-2} pressure. The electrolyte solution (0.6 M

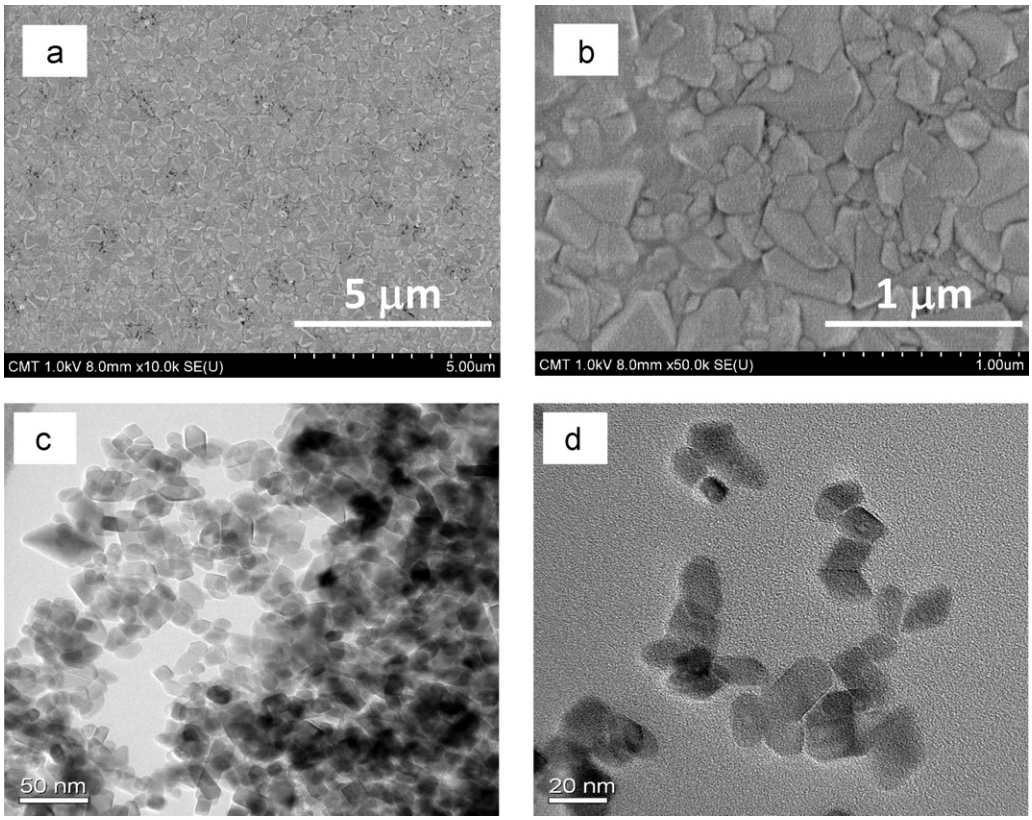

Fig. 1. FE-SEM micrographs of the Pt-electrode at (a) 10k and (b) 50k magnifications, and on TiO_2 nanocrystallines at (c) 50k and (d) 100k magnifications.

PMII/0.05 M I_2/0.1 M LiI/0.5 M TBP in acetonitrile) was injected into one hole on the counter electrode. The holes were sealed using ultraviolet (UV) light after a photo-curing compound was placed in the holes and covered by a slide glass (as shown in Fig. 2(b)).

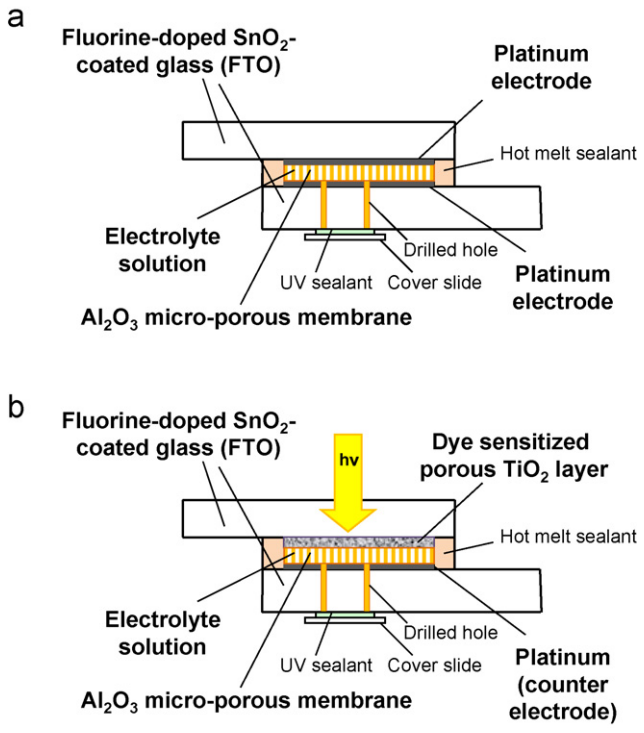

Fig. 2. Cross-sectional illustration of (a) symmetric cell and (b) DSSC.

2.5. Symmetric cell characterization

In the solvent evaporation test, the two drilled holes were not sealed with the photo-curing compound to expedite the drying process. The tested cell was placed on the weight pan of a micro-balance (CP2225D, Sartorius, Goettingen, Germany), and the weight loss was recorded every 15 min.

The limiting current density of the symmetric cell was measured by applying a voltage potential across the electrodes. The scanned potential was varied between −1.0 and 1.0 V at a scan rate of 10 mV s^{-1} using a potentiostat (pgstat3, Autolab, ECO chemie B.V., Utrecht, Netherlands). The limiting current density (J_{lim}) data were used to calculate the I_3^- diffusion coefficients ($D_{I_3^-}$) in the symmetric cells with various Al_2O_3 films [13,14]:

$$J_{lim} = \frac{2nFC_{I_3^-}D_{I_3^-}}{l} \quad (1)$$

where l is the as-measured symmetric cell gap (80 μm), n is charge transfer number in the I^-/I_3^- redox reaction (n = 2 in this case), $C_{I_3^-}$ is the equilibrium concentration of tri-iodide (I_3^-), and F is the Faraday constant.

The charge transfer resistance of the symmetric cell was measured with electrochemical impedance spectroscopy (EIS). The cell was scanned at a frequency between 10^5 and 0.1 Hz and with 10 mV of potential applied across the electrodes. The charge transfer resistances at the Pt-electrolyte interface were determined by analyzing the impedance spectrum and determining the equivalent circuit of the symmetric cells. The Fit and Simulation function in the Frequency Response Analysis mode was performed using the potentiostat, and the individual resistance was extracted. The impedance (in Ω) corresponding to Pt-electrolyte interface (as shown in Section 3.5) was converted to charge transfer resistance (R_{ct}, in Ω cm^2) by taking the active area into consideration. The R_{ct}

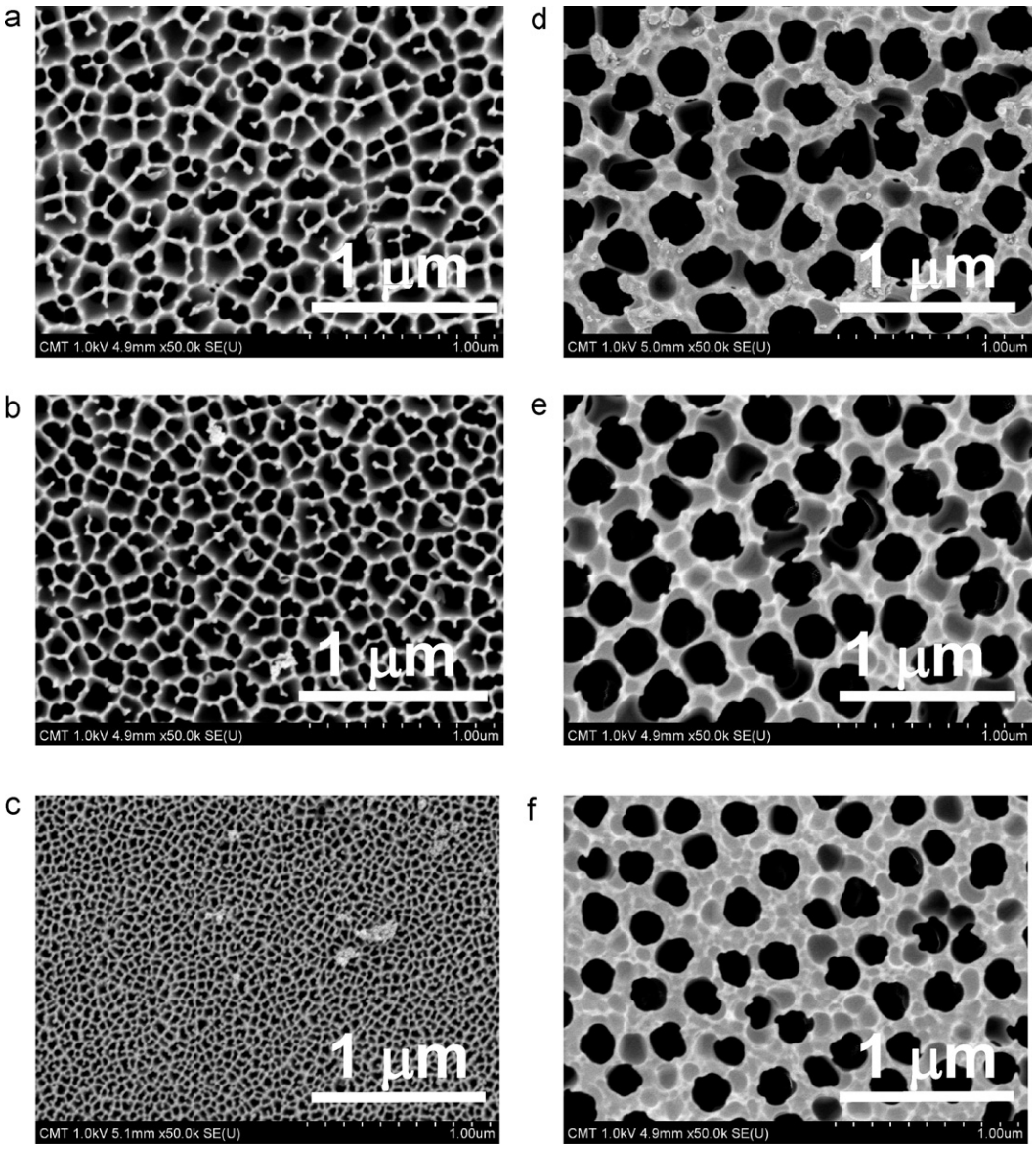

Fig. 3. Surface morphology of different Al_2O_3 membranes with nominal pore sizes of (a) 0.2 μm, top surface; (b) 0.1 μm, top surface; (c) 0.02 μm, top surface; (d) 0.2 μm, bottom layer; (e) 0.1 μm, bottom layer; and (f) 0.02 μm, bottom layer.

value was used to calculate the exchange current density (J_0) in the symmetric cells with various Al_2O_3 films [14].

$$J_0 = \frac{RT}{nFR_{ct}} \tag{2}$$

where R is the gas constant, T is the absolute temperature, n is the charge transport number in each reaction ($n = 2$ in this case), and F is the Faraday constant.

2.6. Photovoltaic efficiency of DSSC

The photo-to-current efficiency of the assembled DSSC was measured using a potentiostat galvanostat (pgstat3, Autolab, Utrecht, Netherlands) with 10^6–10^{-2} Hz and amplitude of 10 mV at 25 °C under 100 mW cm^{-2} illumination (Xenon lamp power supply, model YSS-100A, Yanashita Denso Corp., Tokyo, Japan). The cell was first activated for 20 min and the cell performance data were recorded using the following equations:

$$\eta = \frac{V_{oc} J_{sc}\,\mathrm{FF}}{P_{in}} \times 100\% \tag{3}$$

where η is the photo-to-electric efficiency of DSSC, J_{sc} is the short-circuit current density (the maximum current density value), V_{oc} is the open-circuit voltage (the maximum voltage value), FF is the fill factor, P_{in} is the incident light power. The fill factor is defined as the maximum current density (J) and voltage (V) product value to the $J_{sc}V_{oc}$ product during the measurement:

$$\mathrm{FF} = \frac{(J \times V)_{max}}{J_{sc} \times V_{oc}} \tag{4}$$

3. Results and discussion

3.1. Al_2O_3 ceramic membrane morphologies

The Al_2O_3 ceramic membranes with different nominal pore sizes (0.2, 0.1, 0.02 μm) were characterized to determine their actual

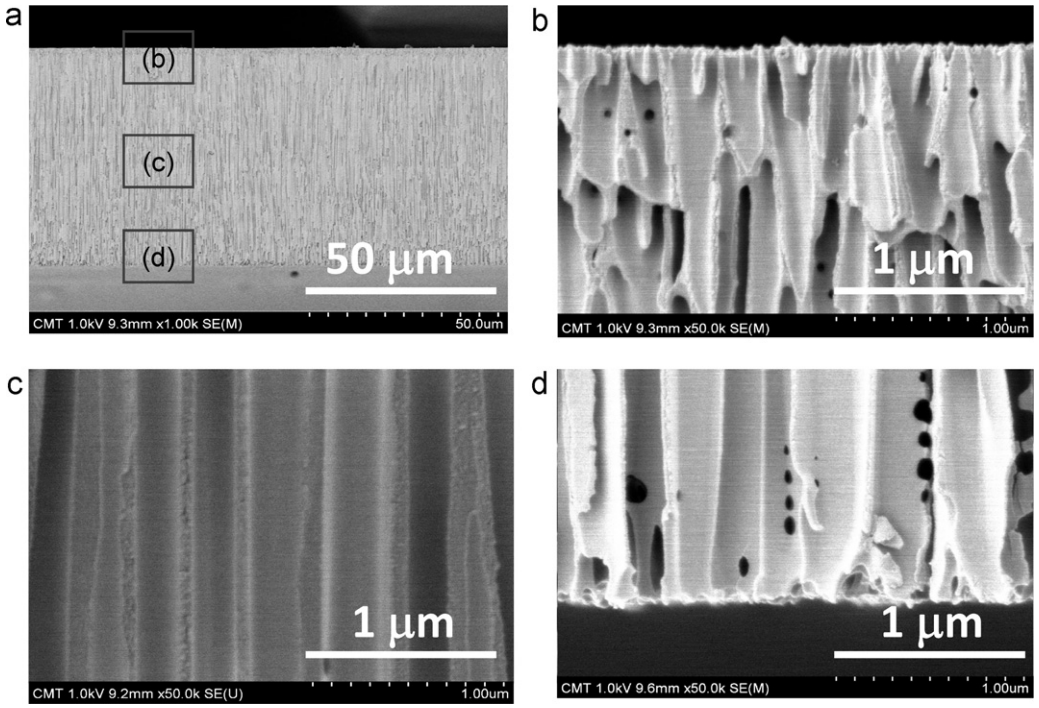

Fig. 4. FE-SEM micrographs of the 0.2-μm Al_2O_3 membrane (a) at 1k magnification for full view, (b) on the top surface at 50k magnification, (c) on the center portion at 50k magnification, (d) on the bottom layer at 50k magnification.

pore sizes, surface morphologies and cross-sectional morphologies using the FE-SEM. The micrographs of the ceramic membranes on both surfaces are shown in Fig. 3. The micrographs indicate that the two surfaces of the ceramic support had different morphologies. The top side had a denser, network-like pore structure, and the pore size was comparable with the nominal size provided by the vendor. The other side exhibited larger apertures that were less dependent on the nominal pore size than the pores on top side.

Fig. 4 shows the cross-sectional structure of the Al_2O_3 ceramic membrane with a pore size of 0.2 μm. The full view and magnified views of the top layer, middle portion, and bottom support layer are shown in (a)–(d), respectively. The images reveal that the thickness of the ceramic film was about 60 μm (Fig. 4(a)). The top surface showed denser structure and more tortuous path (Fig. 4(b)) than the bottom surface. The majority pore structure of the entire cross-section was mainly dominated by the cylindrical open pore structure and parallel pore walls (Fig. 4(c)). The pore opening and geometry of the center part was similar to that of the bottom layer (Fig. 4(d)). The thickness ratio of the top surface to the bottom layer was about 1:29.

The FE-SEM micrographs in Fig. 3 were analyzed using image analysis software. The membrane pore size distribution data for both sides are shown in Fig. 5. At the top surface of the 0.2 μm Al_2O_3 film, 70% of the pores were 0.2 μm in size and the remaining pores were smaller (Fig. 5(a)). At the top surfaces of the 0.1 μm and 0.02 μm Al_2O_3 films, 97% and 81% of the pores had sizes of 0.08 and 0. 2 μm, respectively, with the remaining pores having slightly larger sizes (Fig. 5(b) and (c)). The mean pore sizes at the top surface were 0.180, 0.096, and 0.027 μm, respectively, for the 0.2-, 0.1-, 0.02-μm films (Table 1). More than 90% of the pores on the bottom layers had sizes in the range of 0.2–0.23 μm (Fig. 5(d)–(f)), with average values of 0.23–0.19 μm (Table 1). The thick bottom layer may be used to provide the ceramic membranes with mechanical strength.

The porosity of the membrane was also evaluated using image analysis software. It is defined as the ratio of the total area of the pore voids to the scanned area. The porosity data on both surfaces are shown in Table 1. The porosities were 74%, 70%, and 51% at the top surfaces of the 0.2-μm, 0.1-μm, and 0.02-μm films, respectively. The corresponding porosities at the bottom layers were 66%, 62%, and 41%, for the 0.2-μm, 0.1-μm, and 0.02-μm films respectively. From the results, we can obtain the mean porosity of the each ceramic membrane by normalizing the porosity data to the film thickness, as shown in Table 1. The average porosity value represents the average space available for electrolyte filling and ionic conduction.

3.2. Conductivity of the electrolyte-impregnated ceramic film

The ionic conductivity of the electrolyte-impregnated ceramic film was measured. The electrolyte liquid (control) displayed a conductivity of 25 mS cm^{-1} by direct measurement using a conductivity meter. The conductivities of the ceramic membranes impregnated with the electrolyte solution were determined using electrochemical impedance analysis, and the conductivity data are shown in Fig. 6. The conductivities of the electrolyte-filled ceramic membranes were 9.39 mS cm^{-1}, 8.29 mS cm^{-1} and 6.24 mS cm^{-1}, respectively, for the 0.2-, 0.1- and 0.02-μm Al_2O_3 ceramic membranes. The ionic conductivity seemed to decrease as the pore size of the ceramic membrane decreased. The lower porosity of the smaller pore size membrane may reduce the effective electrolyte holding capacity and the ionic transport pathway, which resulted in the lower ionic conductivity of the electrolyte-filled ceramic membranes. To elucidate the relationship between the ionic conductivity of the Al_2O_3 ceramic membrane impregnated electrolyte and the membrane porosity, Archie's law [15] was employed, as described in the following equation:

$$\sigma_{\text{eff}} = \sigma\, \varepsilon^{m} \tag{5}$$

where σ_{eff} is the effective conductivity, σ is the bulk electrolyte conductivity, ε is the porosity of the Al_2O_3 ceramic membrane, and m is Archie's exponential parameter. The value of m depends on the pore shape of the porous medium. We performed a regression on the experimental conductivity data with Archie's equation and

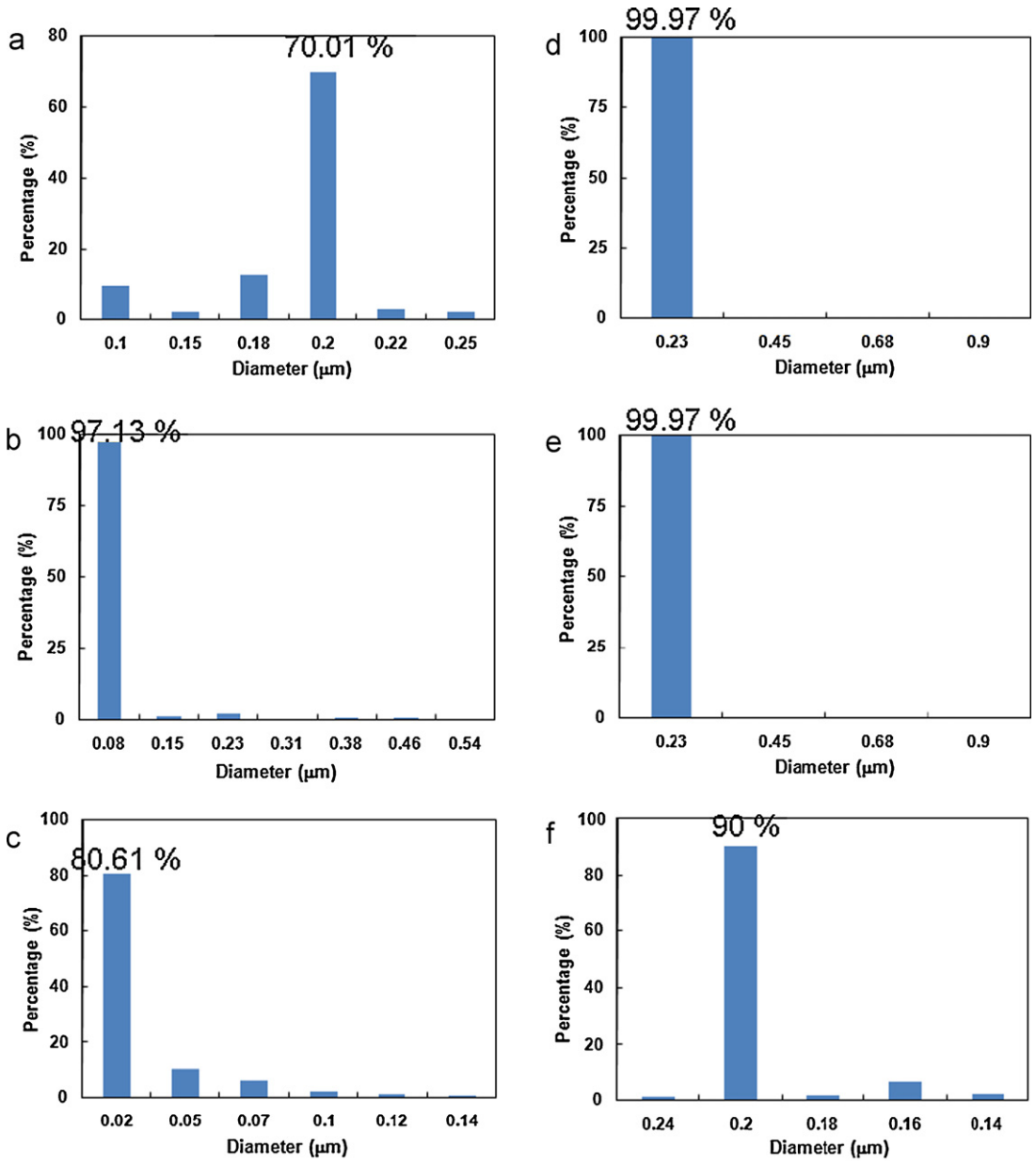

Fig. 5. Pore size distributions for Al_2O_3 membrane supports with nominal pore sizes of (a) 0.2 μm, top surface; (b) 0.1 μm, top surface; (c) 0.02 μm, top surface; (d) 0.2 μm, bottom layer; (e) 0.1 μm, bottom layer; and (f) 0.02 μm, bottom layer.

obtained an m value of 1.811. This fitted result was close to the theoretical value for a porous medium with a cylindrical pore structure, which has an m value of 2 [16]. The finding revealed that the conductivities of Al_2O_3 membranes impregnated with electrolytes were strongly associated with the membrane's pore characteristics. The conductivity can be estimated from the pure electrolyte conductivity, the porosity, and the pore geometry of the porous framework material.

3.3. Solvent evaporation rate with electrolyte-impregnated ceramic film

To investigate the effect of Al_2O_3 on electrolyte retention in the DSSC, we used a symmetric cell without UV sealing on the drilled holes to test the electrolyte solvent evaporation rate at room temperature [6]. The percentage of the solvent weight loss was plotted against the elapsed time, as shown in Fig. 7. We observed

Table 1
Porosities and average pore sizes of different Al_2O_3 ceramic membranes.

Nominal pore size	Porosity (%)		Average porosity[a] (%)	Average pore size (μm)	
	Top	Bottom		Top	Bottom
0.2 μm	74.4	66.0	66.3	0.180	0.230
0.1 μm	70.0	61.7	62.0	0.096	0.228
0.02 μm	51.5	40.6	40.9	0.027	0.186

[a] Calculated as the porosity value from the top and bottom layers, normalized to their thicknesses.

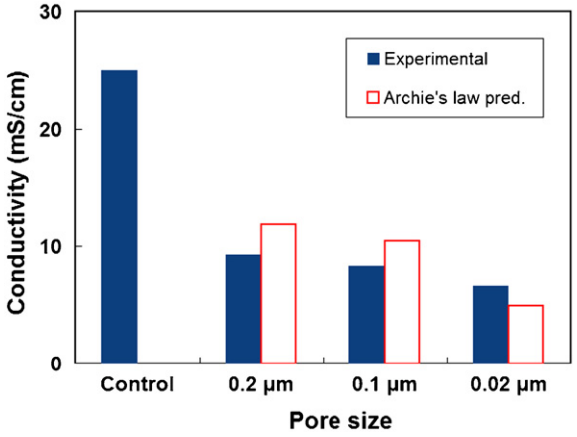

Fig. 6. Ionic conductivity data of different Al_2O_3 membranes with impregnated electrolyte and the estimates using Archie's law regression. (AN electrolyte at 25 °C, membrane thickness: 60 μm).

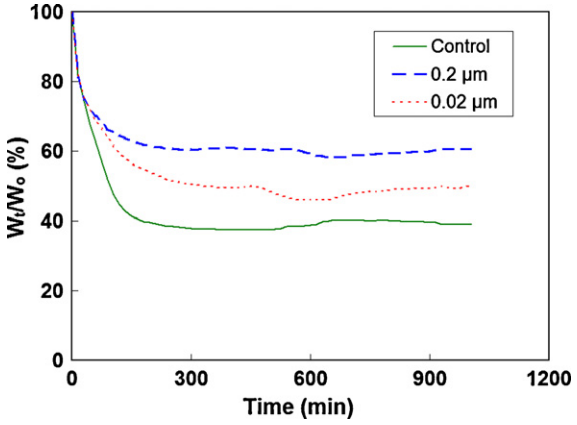

Fig. 7. Electrolyte solvent reduction (relative weight loss) in symmetric cells with Al_2O_3 membranes with nominal pore sizes in the range 0.02–0.2 μm. (AN electrolyte at 25 °C, membrane thickness: 60 μm, W_0 and W_t representing electrolyte weight at initial and at time t).

that in the initial 100 min, electrolyte evaporation occurred in the drilled hole region, and the electrolyte weight decreased dramatically (Fig. 7). This may be due to the electrolyte's direct contact with the atmosphere; therefore, the solvent evaporated much faster there than in the cell gap region. After 100 min, the remaining electrolyte solvent in the gap region had to diffuse through the narrow spaces in the Al_2O_3 film, and the evaporation rate of electrolyte solvent gradually slowed. We found that in the symmetric cells with Al_2O_3 ceramic membranes, electrolyte support significantly suppressed the electrolyte solvent evaporation rate, especially for that with the 0.2 μm pore size. This 0.2-μm film could hold more electrolyte solution due to its higher porosity (66.3% in Table 1) when compared to the 0.02-μm support (40.9% porosity, Table 1). Therefore the evaporation rate was slower in the 0.2-μm film than that with 0.02-μm support (Fig. 7). The pore opening size of 0.2 μm may be sufficient to create capillary force within the pores and retard solvent evaporation [10]. From the measured weight loss changes of the symmetric cells, it can be seen that the inclusion of the micro-porous Al_2O_3 ceramic membrane can effectively reduce the solvent evaporation rate.

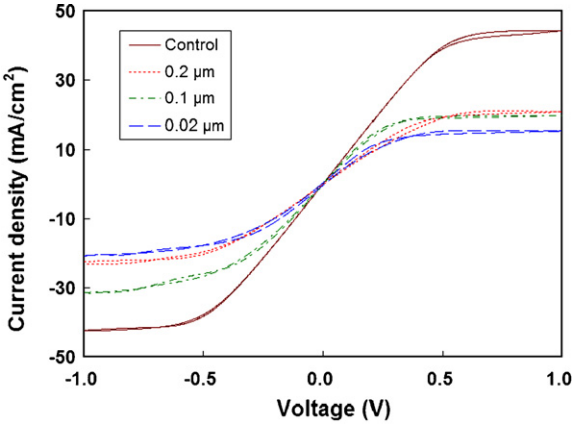

Fig. 8. Cyclic voltammograms of for symmetric cells with electrolyte alone (control) and with Al_2O_3 membranes with nominal pore sizes in the range 0.02–0.2 μm. (AN electrolyte at 25 °C, membrane thickness: 60 μm, cell gap: 65 μm).

3.4. Diffusion coefficient of tri-iodide ions in electrolyte-impregnated ceramic films

In a DSSC, the iodide (I^-, supplied from LiI, PMII) concentration usually exceeds the concentration of I_3^- (formed by LiI and I_2). The I_3^- ion is bulkier and diffuses more slowly than I^-. Therefore, the diffusion behavior of the I_3^- ion is an important factor governing the overall electrolysis current performance (which is a diffusion-limiting step). Here, we used cyclic voltammetry to obtain the limiting current density of the electrolyte system to calculate the diffusion coefficients of I_3^- and to explore the effect of adding Al_2O_3 membranes on the ion transport in the symmetric cell electrolyte system [13]. The limiting current densities (J_{lim}) of the symmetric cells containing different Al_2O_3 membranes are shown as the plateau regimes in Fig. 8. For the control cell (i.e., with acetonitrile solution of 0.1 M LiI/0.6 M PMII/0.05 M I_2/0.5 M TBP), the limiting current density was 44.3 mA cm^{-2}. For comparison, Wang et al. reported a J_{lim} value of 36.1 mA cm^{-2} in a cell containing electrolyte of 0.3 M LiI/0.03 M I_2/0.5 M TBP in acetonitrile [14]. We found that the J_{lim} value decreased to 21.0, 19.6 and 15.6 mA cm^{-2}, respectively, for the cells containing the 0.1-μm, 0.2-μm, and 0.02-μm Al_2O_3 membranes (Table 2). Obviously, the limiting current density of the symmetric cell was correlated with the pore morphology (pore size, porosity, tortuosity, etc.) in the different Al_2O_3 membranes.

We then calculated the I_3^- diffusion coefficient using Eq. (1). The I_3^- diffusion coefficient in the control cell was 1.95×10^{-5} cm^2 s^{-1}. The diffusivity was reduced to 0.92×10^{-5}, 0.86×10^{-5}, and 0.68×10^{-5} cm^2 s^{-1}, respectively, for the cells with 0.1-μm, 0.2-μm, and 0.02-μm Al_2O_3 membranes (Table 2). These data followed a trend that was similar to that followed by the conductivity results of electrolyte-impregnated ceramic films (Fig. 6). In fact, the two data sets had a strong correlation coefficient of 0.9995, indicating that the conductivity value was dominated by the I_3^- diffusion coefficient within the porous membrane. Nevertheless, the I_3^- diffusion coefficient is considered satisfactory compared with the literature data (0.36×10^{-5}–1.6×10^{-5} cm^2 s^{-1} [13,14]) for DSSC applications. The diffusion coefficient should be at least 10^{-6} cm^2 s^{-1} to achieve good performance of the DSSC [13].

3.5. Charge transfer resistance on the Pt-electrolyte interface with an electrolyte-impregnated ceramic film

To further investigate the impact of adding Al_2O_3 membranes on the I_3^- diffusion coefficient, we measured the exchange current density at the Pt and electrolyte interface adjacent to the porous film in

Table 2
Comparison of the limiting current densities, diffusion coefficients of tri-iodide, Pt-electrolyte interface charge transfer resistances and exchange current densities from symmetric cells reported in literature.

Electrolyte	Cell gap (μm)	J_{lim} (mA cm^{-2})	$D_{I_3^-}$ (10^{-5} cm^2 s^{-1})	R_{ct} (Ω cm^2)	J_0 (mA cm^{-2})	Ref.
0.3 M LiI/0.03 M I_2/0.5 M TBP[a] in AN[b]	50	36.1	1.56	1.48	8.69	Wang et al. [14]
0.5 M LiI/0.05 M I_2/10 vol% TBP in AN	20	–	1.4	2.1	–	Hauch and Georg [13]
0.5 M TAPI[c]/0.05 M I_2 in PC[d]	20	-	0.19	17	–	Hauch and Georg [13]
0.5 M LiI/0.05 M I_2/10 vol% TBP in MPN[e]	20	–	0.36	57	–	Hauch and Georg [13]
0.1 M LiI/0.6 M PMII[f]/0.05 M I_2/0.5 M TBP in AN	80	44.3	1.95	1.11	11.5	This work
AN electrolyte[g] with 0.2-μm support	80	21.0	0.92	1.12	11.4	This work
AN electrolyte[g] with 0.1-μm support	80	19. 6	0.86	1.16	11. 1	This work
AN electrolyte[g] with 0.02-μm support	80	15.6	0.68	1.17	11.0	This work

[a] 4-tert-butylpyridine.
[b] Acetonitrile.
[c] Tetrapropyl ammonium iodide.
[d] Propylene carbonate.
[e] 3-Methoxypropionitrile.
[f] 1-Methyl-3-propylimidazolium iodide.
[g] 0.1 M LiI/0.6 M PMII/0.05 M I_2/0.5 M TBP in AN.

the symmetric cells. Generally, I^- is in a large excess relative to I_3^- in the iodide-based liquid electrolyte, and I_3^- is the current-limiting species [13]. The reaction mechanism of the I_3^- ion reduction on the Pt-coated counter electrode plays an important role in the performance of the DSSC. At the counter electrode, I_3^- changes to I^- by gaining two electrons. The other I_3^- ions diffuse from the dye to the counter electrode in the liquid electrolyte solution. Therefore, the charge transfer resistance (R_{ct}) at this electrode is associated with the area fraction of catalyst available for the I^-/I_3^- redox reaction, along with the intrinsic properties of Pt [13]. Electrochemical impedance spectroscopy (EIS) analyses were performed on the symmetric cells [14] to obtain Nyquist plots. Fig. 9 shows a typical impedance spectrum, which was fitted using the equivalent circuit model (which is illustrated in Fig. 9). The first semicircle in the high frequency region (460–100 kHz) was caused by the charge transfer resistance on the Pt-electrolyte interface. The straight line with a slope of ~45° was related to the Warburg impedance at mid-frequency range (1–460 Hz). The low frequency region (0.01–1 Hz) was associated with the infinite diffusion impedance [14]. The analysis reveals that the charge transfer resistance of the symmetric cells with different Al_2O_3 membranes increased slightly as the membrane pore size and porosity decreased: the R_{ct} value increased from the control cell (1.11 Ω cm^2) to the cell with the 0.02-μm film (1.17 Ω cm^2). The dense ceramic top structure may have covered small area on the Pt electrode and resulted in the decreased charge transfer of I_3^-. However, the impact of adding the ceramic film was minor, less than 5% reduction in the R_{ct} value from the control cell.

From the R_{ct} data, we were able to obtain the exchange current density (J_0) at the Pt-electrolyte interface using Eq. (2). The calculated exchange current density values are summarized in Table 2. For the control cell (i.e., with an acetonitrile solution of 0.1 M LiI/0.6 M PMII/0.05 M I_2/0.5 M TBP), the exchange current density was 11.5 mA cm^{-2}. For comparison, Wang et al. reported a J_0 value of 8.69 mA cm^{-2} in a cell containing an electrolyte of 0.3 M LiI/0.03 M I_2/0.5 M TBP in acetonitrile [14]. We found that the J_0 value decreased to 11.4, 11.1 and 11.0 mA cm^{-2}, respectively, for those containing 0.1-μm, 0.2-μm, and 0.02-μm Al_2O_3 membranes (Table 2). Again, the decrease in J_0 due to the incorporation of the ceramic films was limited. The J_0 data in this study were larger than the literature values.

3.6. As-prepared cell performance

Since the Al_2O_3 ceramic membrane had a two-layer structure: a denser top surface and a supporting substrate with different apertures and porosity characteristics, we performed the DSSC tests using the cells with either Al_2O_3 surfaces facing the TiO_2/dye component to examine if any differences were present in their performance. Fig. 10 shows the typical *I–V* curves for the control cell (without ceramic films) and the DSSCs with the various ceramic membranes. The efficiency data in Fig. 11 confirms that the Al_2O_3 membrane orientation did not affect the DSSC performance for cells containing the same ceramic film. The differences were within

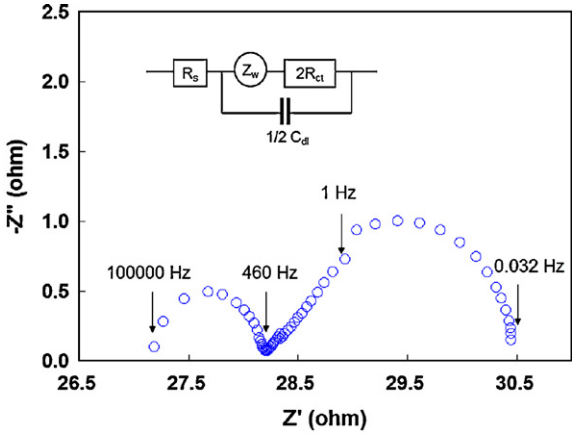

Fig. 9. Typical electrochemical impedance spectrum of symmetric cell based on the equivalent circuit shown in the insert (AN electrolyte at 25 °C, cell gap of 65 μm). The R_s, R_{ct}, Z_w and C_{dl} represent the ohmic serial resistance, charge-transfer resistance, Warburg impedance, and capacitance of electrical double layer, respectively.

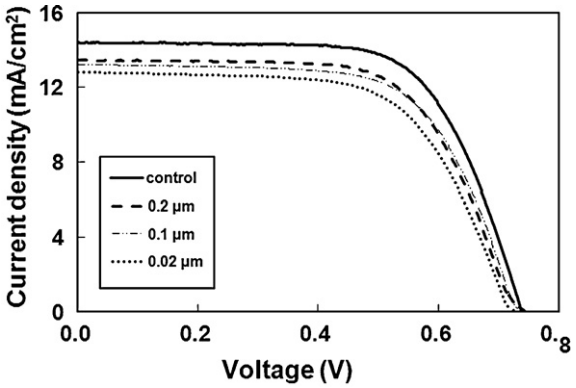

Fig. 10. Photocurrent density–voltage curves for DSSCs assembled with liquid electrolyte and with Al_2O_3 membranes of 0.2 μm, 0.1 μm, and 0.02 μm pore size. The measurements were taken under illumination of 100 mW cm^{-2} (1 sun) after 20 min of activation.

Table 3
Cell performance[a] of DSSCs with and without Al_2O_3 ceramic membrane.

Electrolyte	J_{sc} (mA cm^{-2})	V_{oc} (V)	FF (%)	η (%)
Control	14.4 ± 0.5[b]	0.73 ± 0.01	0.67 ± 0.01	7.13 ± 0.14
0.2 μm	13.5 ± 0.9	0.74 ± 0.01	0.67 ± 0.01	6.67 ± 0.36
0.1 μm	13.2 ± 1.2	0.74 ± 0.01	0.67 ± 0.02	6.46 ± 0.42
0.02 μm	12.8 ± 0.6	0.73 ± 0.01	0.64 ± 0.01	6.01 ± 0.12

[a] Single-sealed cells, operating condition: 25 °C, under illumination of 100 mW cm^{-2} (1 sun).
[b] Mean ± standard deviation (N = 4).

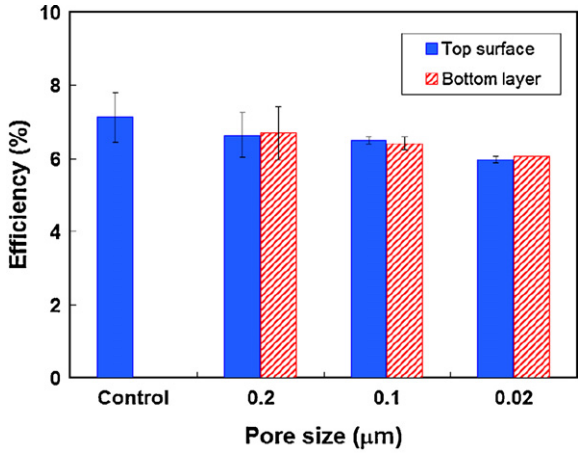

Fig. 11. Light-to-current efficiencies of DSSCs with Al_2O_3 membranes of 0.2 μm, 0.1 μm, and 0.02 μm pore size and the comparison with the control cells (without Al_2O_3 membrane). The cells were fabricated with either top surface or bottom layer (see Figs. 3 and 4 above) facing anode (N = 4).

the experimental error range. The control (without any ceramic support) exhibited slightly higher photo-to-current efficiency compared with the DSSCs with ceramic membranes. We also observed that the efficiency tended to consistently decrease slightly with smaller pore size, as shown in Table 3. The V_{oc} value depends mainly on the redox potential of the electrolyte and the energy difference between the Fermi level of the electrons in the TiO_2 porous layer [17]. In this study, the V_{oc} values were between 0.728 V and 0.743 V and did not show much deviation with each other (Table 3). Similarly the fill factor, between 0.64 and 0.67, hardly changed among the DSSCs with various membranes. The efficiency was strongly correlated with the quantity of the short circuit current density, as reported in the micro-porous polycarbonate-incorporated DSSCs [10].

The data in Fig. 12 and Table 3 show that the photo-to-current efficiency for the control cell was 7.13% and it decreased to 6.01% with the smallest pore size of Al_2O_3 film. This reduction was associated with the decrease in the diffusion coefficient of I_3^- ion and the exchange current density at the Pt-electrolyte interface. From the symmetric cell experiments we show that the I_3^- diffusion coefficient decreased with the decrease in ceramic membrane pore size, reducing the effective I_3^- concentration at the Pt-electrolyte interface and its reduction reaction rate, finally limiting the short circuit density values [18]. The J_{sc} was decreased from 14.4 mW cm^{-2}

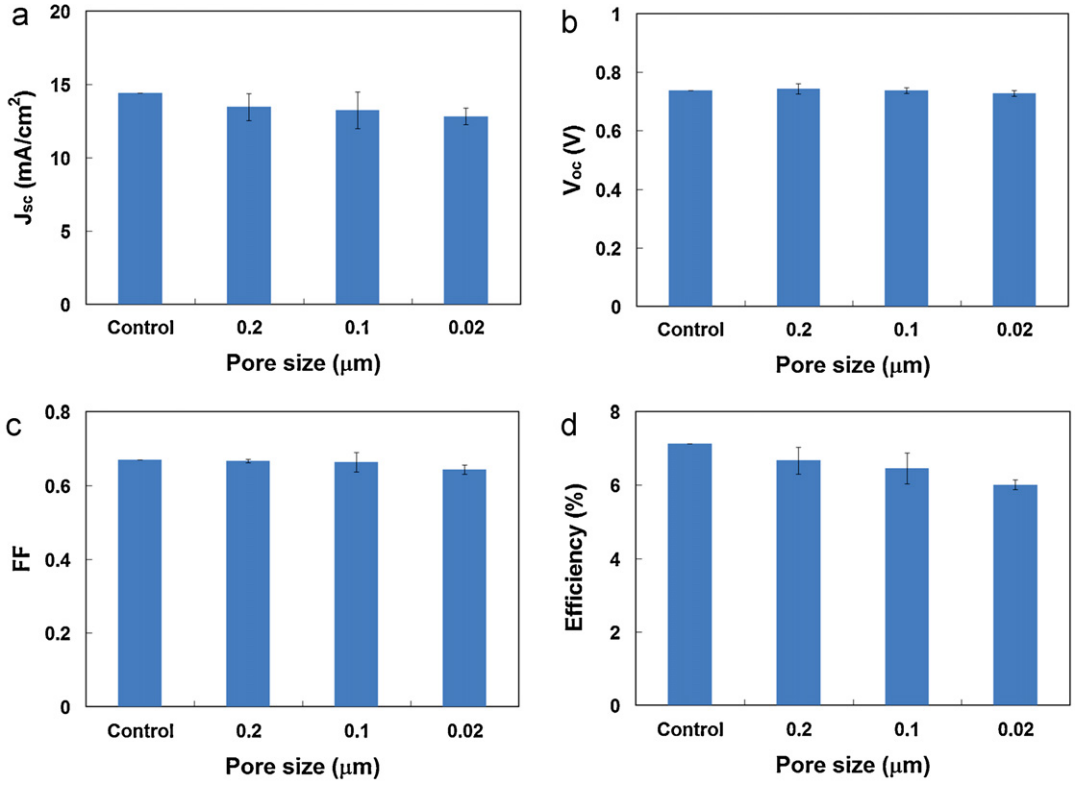

Fig. 12. Means and standard deviations (error bars) of (a) short-circuit photocurrent density, (b) open-circuit voltage, (c) fill factor (FF), and (d) efficiency for as-prepared DSSCs assembled with liquid electrolyte and with Al_2O_3 ceramic membranes. (N = 4, measured at 25 °C under illumination of 100 mW cm^{-2} (1 sun)).

Table 4
Efficiency comparison of DSSCs incorporated with porous framework support to electrolytes.

Porous membrane	Electrolyte	Efficiency (%)	Thickness (μm)	Porosity (%)	Reference
P(AN-MMA)[a]	0.5 M LiI, 0.05 M I_2, 0.05 M TBP[b], AN[c]	2.4 (2.8)[d]	50–60	51	Kim et al. [5]
Polystyrene	0.6 M DMPII[e], 0.1 M LiI, 0.05 M I_2, 0.05 M TBP, 3-MPN[f]	4.58 (4.62)	1.66	27–37	Chen et al. [6]
P(VDF-HFP)/PEG/PEGDMA[g]	0.6 M DMPII, 0.1 M LiI, 0.05 M I_2, 0.05 M TBP, 3-MPN	4.3 (5.1)	12	1–10	Wei et al. [7]
P(VDF-HFP)[h]	0.5 M LiI, 0.05 M I_2, 0.05 M TBP, PC	6.0 (8.6)	30	5-20	Zhang et al. [8]
P(VDF-HFP)[h]	0.6 M BMII[i], 0.03 M I_2, 0.1 M GTC[j], 0.5 M TBP, AN, VN[k]	8 (8)	20	3–5	Park et al. [9]
Polycarbonate	0.6 M PMII [m], 0.1 M LiI, 0.05 M I_2, 0.5 M TBP, AN	5.75 (6.34)	5–6	<10, 0.2-μm[n]	Lue et al. [10]
Al_2O_3	0.6 M PMII, 0.1 M LiI, 0.05 M I_2, 0.5 M TBP, AN	6.67 (7.13) 6.46 6.01	60	66, 0.2-μm[n] 62, 0.1-μm[n] 41, 0.02-μm[n]	This work

[a] Poly(acrylonitrile-methyl methacrylate).
[b] 4-Tert-butylpyridine.
[c] Acetonitrile.
[d] Values in the parentheses are for controlled DSSCs (without porous membranes).
[e] 1,2-Dimethyl-propylimidazolium iodide.
[f] 3-Methoxypropionitrile.
[g] Poly(vinylideneflouride-co-hexafluoropropylene)/polyethylene glycol/polyethylene glycol dimethacrylate.
[h] Poly(vinylideneflouride-co-hexafluoropropylene).
[i] Butylmethylimidazolium iodide.
[j] Guanidinium thiocyanate.
[k] Valeronitrile.
[m] 1-Methyl-3-propylimidazolium iodide.
[n] Pore size.

for the control cell to 12.8 mW cm^{-2} in the 0.02-μm ceramic-containing cell (Table 3).

Table 4 lists the DSSC performance in the literature results, along with the data from this study. Kim et al. prepared acrylonitrile-methyl methacrylate (AN-MMA) co-polymer membrane with a porosity of 51% and film thickness of 50–60 μm [5]. They obtained a photovoltaic efficiency of 2.4% (at 100 mW cm^{-2} illumination) of this DSSC and the control cell had an efficiency of 2.8%. Zhang et al. prepared a smaller area DSSC (0.15 cm^2 compared with 0.25–0.28 cm^2 in other studies) and reported the conversion efficiency of the DSSC with gel membrane was 6.0% at an irradiance of 75 mW cm^{-2}, a lower efficiency than the cell with liquid electrolyte (8.6%) [8]. Chen et al. have shown that the conversion efficiency of 4.58% was obtained with a poly(styrene-methyl methacrylate) (PS-PMMA) blend with a film thickness of only 1.66 μm [6]. Park et al. employed liquid impregnated polymer membranes into DSSC, forming quasi-solid-state electrolytes for highly efficient DSSC with an overall conversion efficiency of 8% at room temperature under

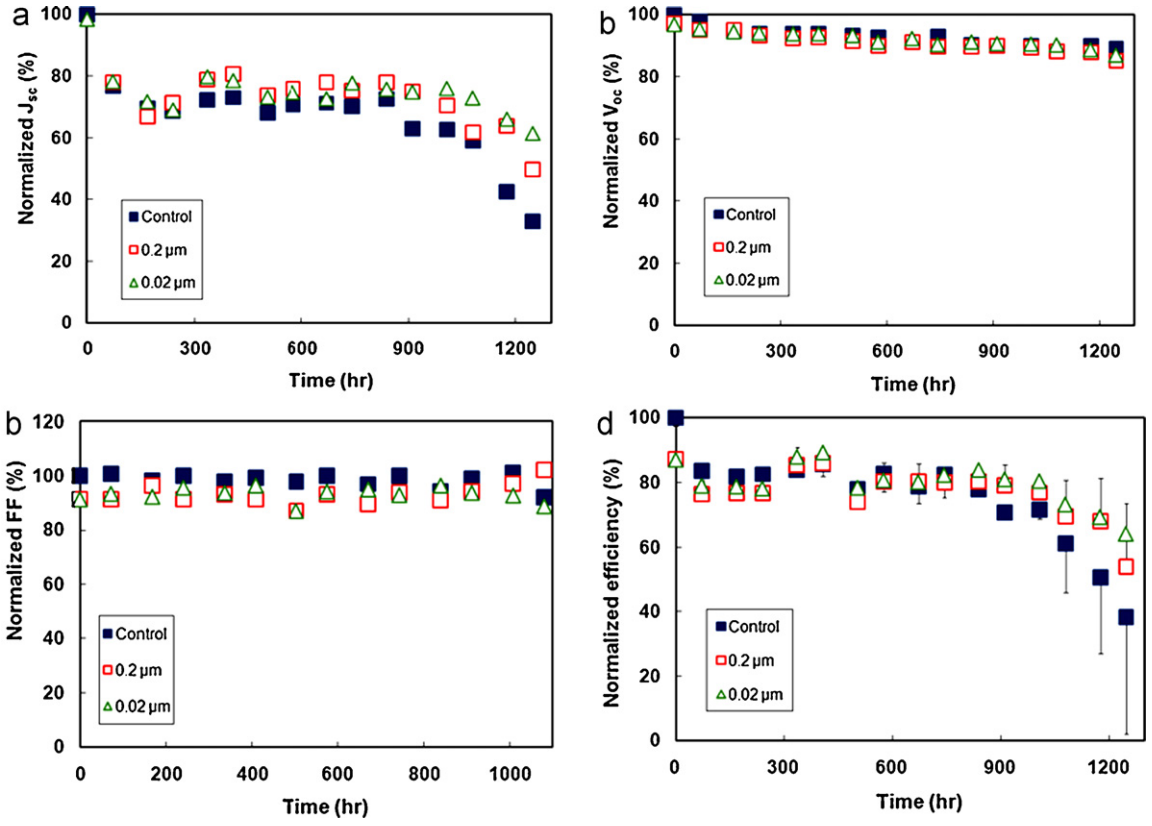

Fig. 13. Normalized values in (a) short-circuit photocurrent density, (b) open-circuit voltage, (c) fill factor (FF), and (d) efficiency as a function of aging time for DSSCs assembled with liquid electrolyte and with Al_2O_3 ceramic membranes. The solar cells were kept in alternating cycles of 3-day light soaking under illumination of 100 mW cm^{-2} (1 sun) and 4-day in-darkness at 25 °C. $N = 3$ for $t = 0$–243 h and $N = 2$ for 240–1248 h).

1 sun illumination [9]. In spite of the fact that our ceramic films were thicker (60-μm) and more porous (66%) than most literature films, sufficient high efficiency of 6.67% and less efficiency reduction from the control cell (from 7.13% to 6.67%) were obtained with the 0.2-μm sample. The ceramic films are chemically and thermally durable and the pore structure is less affected by organic solvent solvation. This may lead to morphology and dimensional stability in the framework material in the DSSC for prolonged use.

3.7. Long-term cell performance

The DSSC with and without Al_2O_3 ceramic membrane as electrolyte support were tested under illumination of 100 mW cm^{-2} (1 sun) at 25 °C in alternating light soaking for 3 days and subsequent 4-day storage at darkness cycles. The relative cell performance results (J_{sc}, V_{oc}, FF, and efficiency divided by the values at time of 0) are shown in Fig. 13. Although the DSSC with Al_2O_3 ceramic membrane had a lower efficiency at the beginning, the cell efficiency was higher than that for the control cell after 840 h (Fig. 13(d)) of alternating sun bathing-darkness cycles. The lesser efficiency drop in the ceramic-containing DSSC was ascribed to the sustained J_{sc} as shown in Fig. 13(a). The Al_2O_3 ceramic membrane exhibited capillary force on the liquid electrolyte within the sub-micro pores and helped with solvent retention. As the DSSC aged, the electrolyte solvent gradually evaporated, resulting in higher internal resistance in the control DSSC. The electrochemical impedance analysis revealed that the combined resistance of the counter electrode and diffusion in the electrolyte in the control DSSC was increased from 7.05 Ω to 11.4 Ω as the time increased from 0 to 1248 h. The DSSC containing 0.2-μm Al_2O_3 had much less resistance increase (from 10.3 Ω to 10.7 Ω) during a similar period. This phenomenon was especially severe at the TCO and Pt-electrolyte interfaces, thus slowing down the J_{sc}. The electrolyte solvent evaporation raised the ion concentrations, which could easily produce dark current at the TiO_2 and electrolyte interface [19], resulting in slight V_{oc} reduction. The fill factor exhibited not much deviation and the cell efficiency was correlated mainly with the J_{sc} value. After 1248 h of aging, the DSSC efficiencies using Al_2O_3 ceramic membranes with 0.2- and 0.02-μm pore size were 4.13% and 4.44%, respectively, accounting for 62% and 74% of their original cell efficiencies (compared at $t = 0$). Conversely, the control cells' efficiency decreased from 7.13% to 2.71% and only 38% of the original efficiency was restored. The inclusion of Al_2O_3 ceramic membrane is beneficial for DSSC life time.

4. Conclusions

This study investigates the electrochemical properties of electrolyte-impregnated micro-porous ceramic (Al_2O_3) films as a framework support for dye-sensitized solar cells (DSSCs). A field-emission scanning electron microscope is used to characterize the morphology on both surfaces of the ceramic membranes, which exhibit high porosity (41–66%) and open cylindrical pore structure. Electrochemical impedance analysis reveals that the conductivity of the electrolyte-impregnated ceramic membranes is lower (6.24–9.39 mS cm^{-1}) than the liquid electrolyte (25 mS cm^{-1}), with an Archie's relationship by a power of 1.81 to the porosity value. The diffusivity of tri-iodide ions (I_3^-) is slowed from 1.95×10^{-5} to 0.68×10^{-5} cm^2 s^{-1} in the ceramic-containing cells. The I_3^- diffusion coefficient is highly correlated with the conductivity of the electrolyte-impregnated membranes, with a correlation coefficient of 0.9995. The exchange current density at the Pt-electrolyte interface is slightly decreased (less than 5%) when Al_2O_3 membranes are used in the symmetric cells, implying that the contact of the denser ceramic top structure on the Pt electrode might not interfere with the I_3^- charge transfer. The ceramic films could prevent solvent evaporation and maintain conductivity in the DSSC. Therefore, the use of these ceramic films as electrolyte framework in DSSC is promising. The long-term cell efficiencies were evaluated up to 1248 h under alternating light soaking and darkness (3 days/4 days) cycles. The cells containing the ceramic films outperformed the control cells.

Acknowledgment

We acknowledge the financial support of the National Science Council of Taiwan (NSC 98-3114-E-182-001-CC2). We would also like to express gratitude to ITRI for technical support in the preparation of the TiO_2, dye solution, and counter electrode.

References

[1] B. O'Regan, M. Grätzel, Nature 353 (1991) 737–740.
[2] S. Yanagida, C. R. Chim. 9 (2006) 597–604.
[3] Y. Yang, C.H. Zhou, S. Xu, H. Hu, B.L. Chen, J. Zhang, S.J. Wu, W. Liu, X.Z. Zhao, J. Power Sources 185 (2008) 1492–1498.
[4] Y. Wang, Y. Sun, B. Song, J. Xi, Sol. Energy Mater. Sol. Cells 92 (2008) 660–666.
[5] D.W. Kim, Y.B. Jeong, S.H. Kim, D.Y. Lee, J.S. Song, J. Power Sources 149 (2005) 112–116.
[6] C.M. Chen, H.S. Shiu, S.J. Cherng, T.C. Wei, J. Power Sources 188 (2009) 319–322.
[7] T.C. Wei, C.C. Wan, Y.Y. Wang, Sol. Energy Mater. Sol. Cells 91 (2007) 1892–1897.
[8] X. Zhang, C.X. Wang, F.Y. Li, Y.Y. Xia, J. Photochem. Photobiol., A 194 (2008) 31–36.
[9] J.H. Park, Y.C. Nho, M.G. Kang, J. Photochem. Photobiol., A 203 (2009) 151–154.
[10] S.J. Lue, P.W. Lo, L.Y. Hung, Y.L. Tung, J. Power Sources 195 (2010) 7677–7683.
[11] S.J. Lue, J.J. Hsu, T.-C. Wei, J. Membr. Sci. 321 (2008) 146–154.
[12] S.J. Lue, W.T. Wang, K.P.O. Mahesh, C.-C. Yang, J. Power Sources 195 (2010) 7991–7999.
[13] A. Hauch, A. Georg, Electrochim. Acta 46 (2001) 3457–3466.
[14] N. Wang, H. Lin, X. Li, C. Lin, L. Zhang, J. Wu, Y. Dou, J. Li, Electrochem. Commun. 8 (2006) 946–950.
[15] J.N. Roberts, L.M. Schwartz, Phys. Rev. B: Condens. Matter Mater. Phys. 31 (1985) 5990–5997.
[16] P. Grathwohl, Diffusion in Natural Porous Media, second Edn, Kluwer Academic Publishers, Boston, USA, 2000.
[17] A. Hagfeldt, M. Grätzel, Chem. Rev. 95 (1995) 49–68.
[18] T. Asano, T. Kubo, Y. Nishikitani, J. Photochem. Photobiol., A 164 (2004) 111–115.
[19] S.Y. Huang, G. Schlichthor, A.J. Nozik, M. Grätzel, A.J. Frank, J. Phys. Chem. B 101 (1997) 2576–2582.